INTERNATIONAL JOURNAL FOR NUMERICAL METHODS IN FLUIDS
Int. J. Numer. Meth. Fluids 2001; **35**: 961–982

A front-capture scheme for the simulation of homogeneous and particle-laden gravity currents

William A. Engblom[a,b,*,1], Larry W. Lake[a] and Roger T. Bonnecaze[b]

[a] *Department of Petroleum and Geosystems Engineering, The University of Texas at Austin, Austin, TX, U.S.A.*
[b] *Department of Chemical Engineering, The University of Texas at Austin, Austin, TX, U.S.A.*

SUMMARY

This paper presents a new finite volume scheme to efficiently simulate gravity currents flowing over complex surfaces. The two-dimensional shallow-water equations, with terms to account for friction and particle transport, are solved using a non-oscillatory technique. By applying a form drag at the front or head of the dense current, the scheme also implicitly captures the correct Froude number condition at the moving front as it intrudes into the less dense ambient fluid. The Froude number of the head region predicted by the numerical simulation is in good agreement with experimental results for a homogeneous current over a horizontal surface if a realistic profile drag coefficient is chosen. This new scheme avoids the development complexities of a general front-tracking scheme (e.g., handling merging fronts and multiple currents) and the computational cost of solving the full three-dimensional Euler equations while providing a fast, accurate simulation of gravity currents. Copyright © 2001 John Wiley & Sons, Ltd.

KEY WORDS: finite volume; front capture; gravity flow; non-oscillatory; particle transport

1. INTRODUCTION

Gravity currents are important in many environmental and geological processes: sediment deposition, structure safety evaluation and pollutant transport are only a few of its applications [1]. Our interest is primarily in sediment transport in naturally occurring gravity of so-called turbidity flows, particularly for the formation of the oil-bearing turbiditic rocks [2,3]. Figure 1 depicts the formation of a sediment layer within a turbiditic reservoir caused by a landslide. Specifically, an unstable portion of the shelf slides down the shelf, entrains water and forms a dense suspension which then spreads across the basal surface. The current can deposit sediment and cut channels as it travels.

Gravity currents are dense regions of fluid and sediment intruding into a less dense ambient fluid. Gravity currents have a blunt nose or head followed by a thin, usually quite long, region

* Correspondence to: The Aerospace Corporation. PO Box 92957-M4/964, Los Angeles, CA 90009-2957, U.S.A.
[1] E-mail: William.A.Engblom@aero.org

Received 12 July 1999
Revised 18 June 2000

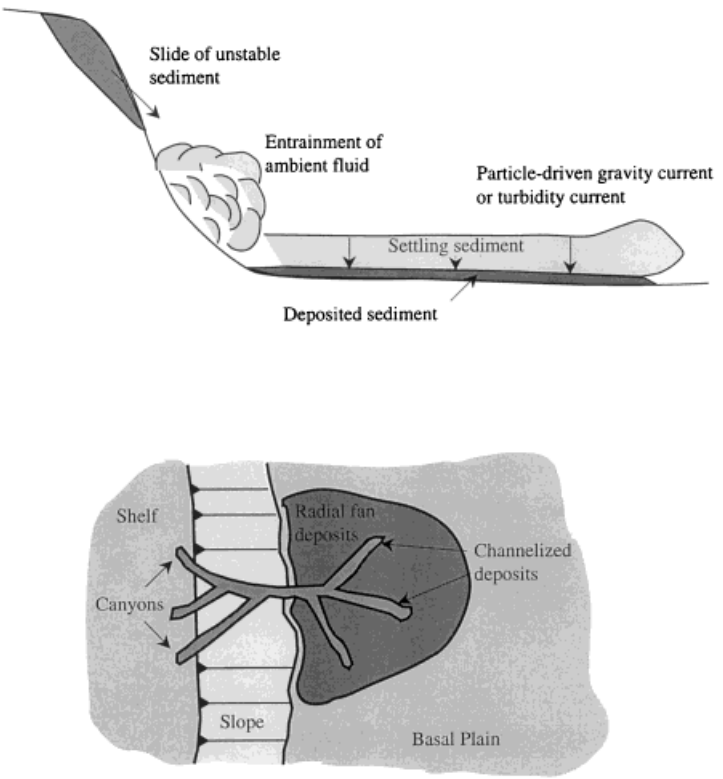

Figure 1. Schematic of turbidite formation.

back to the current source. The density difference (or buoyancy force) driving the motion may be the result of different compositions or temperatures of the fluids of the gravity current and ambient environment. Particle-laden turbidity currents contain a suspension of particles that makes the bulk density of the current greater than that of the ambient fluid. As these currents proceed, the particle concentration decreases because of deposition, causing the current to slow and eventually stop. This motion (and several repetitions of it) leaves behind a region of deposited particles over a basal surface that can subsequently form a hydrocarbon-bearing reservoir.

The most important gravity currents for the deposition of hydrocarbon-bearing turbidites occur at the margins of continental shelves. These currents leave remnants that can extend several kilometers into the deeper sea floor. The extent and depth of these deposits are of great interest for the search and exploitation of the hydrocarbon-bearing reservoirs. The geometry of these deposits depends on several factors, including the topography of the sea floor.

The purpose of the present paper is to develop an efficient, robust and reliable method for numerical simulation of gravity currents and to use the simulator to gain insight into the

physics of particle-driven gravity flows over an arbitrary surface. Specifically, we present a numerical method that accurately and efficiently describes the flow of the gravity current over an arbitrary topography. Our simulation is based on a new method for capturing the front as it intrudes into the ambient fluid.

The dynamics of the front of a gravity current were originally studied by Von Karman [4] and Benjamin [5], who showed that the velocity of the front U_f is proportional to the local shallow-water wave speed, or $U_f = Fr(g'H_f)^{1/2}$, where H_f is the height of the front and Fr is the proportionality constant or Froude number, and g' is reduced gravity given by $g' = g(\rho_c - \rho_a)/\rho_a$, where ρ_c and ρ_a are the densities of the current and ambient respectively, and g is the gravitational acceleration. Theoretically, they predicted $Fr = \sqrt{2}$, but experimentally it is found that $Fr = 1.19$ for a constant volume release [6]. The discrepancy is probably because of additional Reynold stresses not accounted for in the theory.

The dynamics and deposition of two-dimensional and axisymmetric particle-laden currents have recently been studied by Bonnecaze *et al.* [7–9] and Sparks *et al.* [10]. They describe the flow of the particle-laden currents using the shallow-water equations and an additional equation for the transport and settling of particles. The model assumes the particles to be vertically well mixed because of turbulence. At the front of the current the Froude condition is enforced. The numerical solution to this non-linear moving front problem is in excellent agreement with the laboratory experiments. Bonnecaze and Lister [11] have recently applied the model to the constant flow of a particle-laden gravity current down a planar slope, with the addition of friction and entrainment of ambient fluid. Particularly useful in this last study, and in Bonnecaze *et al.* [9], were various scaling analyses that predicted the extent and depth of a deposit based on the size of the initial charge, its concentration of particles, the settling velocity of the particles, the slope and the friction and entrainment coefficients.

In this paper we develop a simulation of the dynamics of and deposition from a gravity current that is the result of a fixed volume release of particle-laden fluid flowing over an arbitrary surface. First, we present the shallow-water equations for quasi-three-dimensional flow of the current, including the effects of friction and the advection and settling of one or several sizes of particles. A non-oscillatory, finite volume method is described for integration of the non-linear partial differential equations (PDEs). Added to this is a method for front capture that imposes a form drag at the front. This effectively captures the appropriate Froude condition at the front of the current but without explicitly imposing it. Capturing the front based on appropriate fluid physics rather than imposing a single Froude condition is a necessary step towards a general, gravity current simulation capability. Another advantage of the new method is that it can naturally model the merging of two fronts without the need for an additional algorithm. The simulation is then applied to a few sample cases to demonstrate its performance and robustness.

2. THEORY

The shallow-water equations (SWE) for two-dimensional (quasi-three-dimensional) particle-driven currents are given below in integral (conservative) form. These equations state that the time rate of change of the mass and momentum within a two-dimensional control surface (S)

along the basal surface plus the flux of these quantities through the control surface boundary (C) is equal to any additional sources of mass and momentum. U is the conservative state vector, $\bar{P}$ is the flux tensor and N is the source vector

$$\frac{\partial}{\partial t}\iint_S U\cdot \mathrm{d}S + \oint_C \bar{P}\cdot\bar{n}\,\mathrm{d}C = \iint_S N\cdot \mathrm{d}S \tag{1}$$

The SWE for particle-driven currents include conservation equations for ambient fluid mass, solid particle mass, x-momentum and y-momentum, where the x- and y-directions are orthogonal and along the basal floor respectively. The conservative state vector is a function of ϕ (particle volume fraction), h (fluid height), u (x velocity) and v (y velocity). The current density (ρ_c) is a function of ϕ, ambient fluid density (ρ_a) and particle density (ρ_p). Note that the equations assume one particle type or 'specie' but can easily be extended to multiple particle species

$$U = \begin{bmatrix} h(1-\phi) \\ h\phi \\ \rho_c hu \\ \rho_c hv \end{bmatrix} \tag{2}$$

where $\rho_c = \rho_a(1-\phi) + \rho_p\phi$.

The flux tensor $\bar{P}$ separates into the F and G components that correspond to the x- and y-directions respectively. The additional term, p, is the force due to the integration of hydrostatic pressure over the current height

$$\bar{P} = F\hat{i}_x + G\hat{i}_y \tag{3}$$

where

$$F = \begin{bmatrix} h(1-\phi)u \\ h\phi u \\ \rho_c hu^2 + p \\ \rho_c huv \end{bmatrix}, \qquad G = \begin{bmatrix} h(1-\phi)v \\ h\phi v \\ \rho_c huv \\ \rho_c hv^2 + p \end{bmatrix}$$

where $p = (\rho_c - \rho_a)gh^2/2$.

The source term N accounts for the effects of particle deposition (N_{deposit}), slope (N_{slope}), bed friction (N_{friction}) and profile drag (N_{profile}). More specifically, N_{deposit} accounts for the deposition of solid particles to the bed floor and entrainment of ambient fluid through the top of the current. The deposition term is a function of particle size via particle settling velocity (V_s). N_{slope} is the component of the fluid weight that is oriented along the floor. N_{friction} accounts for the drag losses along the floor and is estimated based on the empirical formula from Manning [12]. N_{profile} is the profile drag exerted by the ambient fluid on the intruding gravity current. N_{profile} will be discussed later since it only applies to the front-capture method

$$N = N_{\text{deposit}} + N_{\text{slope}} + N_{\text{friction}} + N_{\text{profile}} \tag{4}$$

where

$$N_{\text{deposit}} = \begin{bmatrix} +V_s\phi \\ -V_s\phi \\ (\rho_a - \rho_p)V_s u\phi \\ (\rho_a - \rho_p)V_s v\phi \end{bmatrix}, \qquad N_{\text{slope}} = \begin{bmatrix} 0 \\ 0 \\ -(\rho_c - \rho_a)gh\dfrac{\partial z}{\partial x} \\ -(\rho_c - \rho_a)gh\dfrac{\partial z}{\partial y} \end{bmatrix},$$

$$N_{\text{friction}} = \begin{bmatrix} 0 \\ 0 \\ -(\rho_c - \rho_a)gh\dfrac{n^2 u\sqrt{u^2+v^2}}{h^{4/3}} \\ -(\rho_c - \rho_a)gh\dfrac{n^2 v\sqrt{u^2+v^2}}{h^{4/3}} \end{bmatrix}$$

For a more detailed discussion of the governing equations for particle-driven flows see Bonnecaze *et al.* [7,9] and Bonnecaze and Lister [11].

3. NUMERICAL METHOD

Numerical simulations for one- and two-dimensional axisymmetric, homogeneous and inhomogeneous gravity currents over level surfaces have been presented by Bonnecaze *et al.* [7,8]. Their simulations employed the SWE equations with particle deposition (Equation (1)–(4)) and imposed a Froude condition at the current front. Their simulations predicted the shape of the current, the position of the front versus time, and particle mass deposition contours of corresponding experiments. The numerical schemes in their studies used a finite difference Lax–Wendroff method with one-dimensional adaptable grids where the motion of the front is calculated based on one-dimensional characteristics. Such an approach includes the fixed *Fr* condition explicitly.

This work uses a finite volume method for the integration of the two-dimensional SWE. The control volume equations (1) are integrated in time using the explicit, second-order Runge–Kutta (RK) scheme given below. This two-stage RK scheme preserves the total variation diminishing (TVD) property under specific Courant–Friedrichs–Lewy (CFL) restrictions, as shown by Shu and Osher [13]

$$U^p_{i,j} = U^n_{i,j} - \Delta t\left[\left(\frac{f^n_{i+1/2,j} - f^n_{i-1/2,j}}{\Delta x}\right) + \left(\frac{g^n_{i,j+1/2} - g^n_{i,j-1/2}}{\Delta y}\right) + N^n_{i,j}\right]$$

$$U_{i,j}^{n+1} = 0.5\left[U_{i,j}^{n} + U_{i,j}^{p} - \Delta t\left[\left(\frac{f_{i+1/2,j}^{p} - f_{i-1/2,j}^{p}}{\Delta x}\right) + \left(\frac{g_{i,j+1/2}^{p} - g_{i,j-1/2}^{p}}{\Delta y}\right) + N_{i,j}^{p}\right]\right] \tag{5}$$

A significant issue is numerical stability within thin regions of a gravity current (behind the bulbous head in Figure 1). Solutions to the SWE are unstable when the height of the current reaches zero. Spurious oscillations in the solution, which occur because of the numerical formulation, can cause the current height to be negative in these thin regions. Consequently, numerical oscillations must be minimized.

Many high-resolution schemes have been proposed for solving the SWE. These schemes typically produce minimal spurious oscillations and are computationally expensive. However, for cases involving complex surfaces (i.e., a source term), these schemes may produce significant oscillations [14]. Nessyahu and Tadmor [15] demonstrated that the more robust and simple Lax–Friedrichs solver, with artificial viscosity and high-resolution MUSCL-type interpolants, can provide adequate spatial accuracy while eliminating oscillations and reducing computational effort. Nujic [14] demonstrated that the Lax–Friedrichs scheme with a separate numerical treatment of the source and pressure terms produces negligible oscillations, even for cases with complex topographies.

We chose a numerical discretization based on Nujic's scheme to minimize spurious oscillations. Specifically, all terms except the particle deposition and profile drag source terms are discretized based on the non-oscillatory (NO) scheme developed by Nujic [14]. Specifically, the mass and momentum fluxes within F and G at each cell face (e.g., $f_{i+1/2}$) are calculated from the simple Lax–Friedrichs (LF) function. Spatially second-order fluxes from the left and right sides of the face (i.e., f_{L} and f_{R}) are calculated based on extrapolated state vector values, u_{L} and u_{R}

$$f_{i+1/2} = 0.5[f_{\mathrm{R}} + f_{\mathrm{L}} - \alpha_{i+1/2}(u_{\mathrm{R}} - u_{\mathrm{L}})] \tag{6}$$

where

$$f_{\mathrm{L}} = f(u_{\mathrm{L}}), \qquad f_{\mathrm{R}} = f(u_{\mathrm{R}}), \qquad u_{\mathrm{L}} = u_i + 0.5\delta u_i, \qquad u_{\mathrm{R}} = u_{i+1} - 0.5\delta u_{i+1}$$

These state vector values are further limited by a minmod function to reduce oscillations

$$\delta u_i = \mathrm{minmod}(u_{i+1} - u_i, u_i - u_{i-1})$$

$$\delta u_{i+1} = \mathrm{minmod}(u_{i+1} - u_i, u_i - u_{i-1}) \tag{7}$$

The LF function is fast and produces similar results to more complex functions provided the numerical dissipation is chosen carefully. Too much dissipation produces smeared results while too little leads to spurious oscillations. Consequently, one must check the sensitivity of the solution to the dissipation function. In the present scheme, a conservative level of dissipation is calculated at each cell face from the local maximum eigenvalue (λ_j) over m points defined by the stencil for each particular face, as suggested by Nujic [14]. That is, the present numerical scheme limits accuracy to ensure stability. A discussion of the eigenvalue system for the homogenous SWE may be found in Reference [18]

$$\alpha_{i+1/2} = \max|\lambda_j|, \quad j = 1, \ldots, m \tag{8}$$

The integrated pressure (p), slope (N_{slope}) and friction (N_{friction}) source terms are central-differenced to promote numerical compatibility [14]. Here z is the local depth of the basal floor. Equation (9) includes discretizations for the x-momentum equation only, for brevity. The source term associated with particle deposition (N_{deposit}) is calculated directly from the local cell values, for simplicity (not shown)

$$p_{i+1/2,j} = \frac{(p_{i+1,j} + p_{i,j})}{2}$$

$$N_{\text{slope}} = -(\rho_c - \rho_a) g (h_{i+1,j} + h_{i-1,j}) \frac{(z_{i+1,j} - z_{i-1,j})}{2\Delta x}$$

$$N_{\text{friction}} = -(\rho_c - \rho_a) \times g \frac{\left(h_{i+1,j} \dfrac{n^2 u_{i+1,j} \sqrt{u_{i+1,j}^2 + v_{i+1,j}^2}}{h_{i+1,j}^{4/3}} + h_{i-1,j} \dfrac{n^2 u_{i-1,j} \sqrt{u_{i-1,j}^2 + v_{i-1,j}^2}}{h_{i-1,j}^{4/3}} \right)}{2} \tag{9}$$

Even though the proposed scheme was adapted from Nujic's NO scheme, it is not clear whether it can still be classified as NO. The introduction of numerical 'inhomogenities', such as complex topography, particle deposition and profile drag, into the scheme can cause oscillations. This subtlety will be explored in future efforts.

The numerical treatment of the profile drag term (N_{profile}) for the proposed numerical scheme will be addressed later in Section 5. Note that the innovation of the proposed scheme is in the front-capture technique (i.e., the boundary condition treatment), not the NO numerical scheme. The 'unique' fluid physics at the current head require special treatment, which cannot be addressed via the SWE. For a proper perspective, it is useful to first review the front-tracking approach.

4. FRONT-TRACKING SCHEME

At first a 'classical' front-tracking scheme, based on the work of Chern *et al.* [16], was developed to simulate the evolution of the front of the gravity current. This technique involves two grids: a fixed two-dimensional Cartesian grid, which contains the entire flow domain, and a one-dimensional grid (i.e., piecewise linear curve) to track the boundary between the current and the ambient fluid. The interior current flow is calculated using the control volume formulation discussed earlier in Section 2, with the exception of the profile drag source term. These conservation equations are also discretized similarly to the scheme described in Section 3, except that van Leer flux-splitting with MUSCL was applied to the F and G components of the flux tensor. The major difference between the front-tracking and front-capture schemes is in the treatment of the current front.

The change in the fluid state in the Cartesian cells that are 'cut' by the interface is calculated based on a deformable control volume formulation. Consequently, the first term on the left-hand side of Equation (1) must be modified to account for the effect of area change. A spatially second-order, temporally first-order accurate discretization of the governing equations may be obtained as follows:

$$U_{i,j}^{n+1} = \frac{(U_{i,j}^{n} \cdot A_{i,j}^{n} + \bar{U}_{\text{front}}^{n} \cdot (A_{i,j}^{n+1} - A_{i,j}^{n}))}{A_{i,j}^{n+1}} - \frac{\Delta t}{A_{i,j}^{n+1}} (R_{i,j}^{n} + N_{i,j}^{n} \cdot A_{i,j}^{n+1}) \tag{10}$$

where

$$R_{i,j}^{n} = f_{i+1/2,j}^{n} \cdot \Delta y_{i+1/2,j}^{n} - f_{i-1/2,j}^{n} \cdot \Delta y_{i-1/2,j}^{n} + g_{i,j+1/2}^{n} \cdot \Delta x_{i,j+1/2}^{n} - g_{i,j-1/2}^{n} \cdot \Delta x_{i,j-1/2}^{n}$$

Here $\bar{U}_{\text{front}}$ is an appropriate state vector value for the interface segment(s) which cut the cell. The fluid state at the 'cut' or interface is estimated based on the solution to a local one-dimensional Riemann problem in which the characteristics are assumed normal to the front. Specifically, the fluid state (i.e., height and velocity) at the current interface is extrapolated from the interior based on two equations: (1) the only outward-going characteristic; and (2) a supercritical Froude number constraint (e.g., 1.2). Density variations are neglected at the boundary since, because of turbulent mixing, large 'jumps' or discontinuities in current density are not physically reasonable inside the current. The effect of the slope source term at the boundary is omitted in this step for simplicity, although this almost certainly introduces some error. It should be emphasized that the Froude condition at the interface is imposed to reproduce the 'unique' flow behavior at the current head.

The position of the piecewise linear interface is integrated according to the extrapolated fluid states along the front (i.e., velocities). Consequently, the local cell area included within the current, A, in Equation (10) will change as the current front passes over the cell. The residual, R, represents the fluxes through each face of the Cartesian cell. Note that some of the Δx and Δy values will be fractions of the cell face lengths, depending on the how the cell is cut by the interface segments. If a local cell area A is too small the deformable control volume formulation in Equation (10) is not suitable [16]. As the current passes into a new cell the fluid state is initially approximated from nearby states on the front. Once the current has passed completely over a cell, the non-deformable control volume formulation is recovered ($A_{i,j}^{n+1} = A_{i,j}^{n}$; Δx and Δy are their maximum grid value).

This front-tracking technique works well for simple problems (e.g., axisymmetric currents over a horizontal slope). Near-perfect agreement between the results of this code and the numerical work of Bonnecaze *et al.* [7,8] was obtained for two-dimensional and axisymmetric turbidity currents (both homogeneous and non-homogeneous cases) over horizontal surfaces.

However, adapting the front-tracking method to handle complex surfaces with front merging is excessive. This scheme lacked robustness in cases involving all but the simplest basal surfaces because the local characteristics at the current head tended to cross each other during a time step. And the compensating adjustment of the flow cells caused a loss of closure in the material balance.

We did, in fact, perform several complicated simulations, but each simulation required a significant effort to coax it to completion. This experience suggested that a front-capturing scheme, which appropriately addresses the physics near the current head, would be highly desirable. How we deal with this is a major novelty of this work. We use the tracking method, described above, to generate results for horizontal surface cases that are used to validate the new *front-capturing* code.

5. PROPOSED FRONT-CAPTURE METHOD

The main idea behind the new scheme is to model the dynamics of the current head based on the assumption that the Froude condition can be described by a form drag acting on the bulbous head of the front. This scheme diffusely captures the front, thus avoiding the requirement for the front-tracking approach. We do this by specifically adding a form drag component to the N-vector for the momentum balances of the fluid to account for the hydrodynamic pressure (or profile) drag exerted by the ambient fluid on the current head. This source term is applied to all cells within the domain; however, the magnitude tends to be significant only along the current head.

This hydrodynamic profile drag (N_{profile}) is calculated conventionally based on an appropriate drag coefficient (C_{D}), dynamic pressure (Q) and exposed surface area (S). As discussed later, we used a range of physically appropriate drag coefficients (C_{D}) based on the typical shape of a gravity current head. Q depends on the total relative velocity between the current and ambient fluid (V_{r}), and the density of the ambient fluid (ρ_{a}). S is the surface area exposed to the relative 'wind'. This surface area is simply the dot product of the gradient vector of current height along the floor and the relative velocity direction vector, multiplied by the cell area (A). Note that the relative velocity (V_{r}) is identical to the local velocity vector, assuming the surrounding ambient fluid 'far-field' is at rest.

$$N_{\text{profile}} = \begin{bmatrix} 0 \\ 0 \\ C_{\text{D}} Q S \dfrac{u}{V_{\text{r}}} \\ C_{\text{D}} Q S \dfrac{v}{V_{\text{r}}} \end{bmatrix} \tag{11}$$

where

$$Q = \frac{\rho_{\text{a}} V_{\text{r}}^2}{2}, \qquad S = \left(\frac{u}{V_{\text{r}}} \cdot \frac{\partial h}{\partial x} + \frac{v}{V_{\text{r}}} \cdot \frac{\partial h}{\partial y} \right) A, \qquad V_{\text{r}} = \sqrt{u^2 + v^2}$$

The N_{profile} term is discretized using central differencing (shown below), consistent with the treatment of the pressure, slope and bed friction terms. Recall that the entire numerical scheme, excluding the profile drag term, has been described earlier in the Section 3

$$N_{\text{profile}} = \begin{bmatrix} 0 \\ 0 \\ 0.5C_{\text{D}}\rho_{\text{a}}S(\sqrt{u_{i,j}^2 + v_{i,j}^2}u_{i,j}) \\ 0.5C_{\text{D}}\rho_{\text{a}}S(\sqrt{u_{i,j}^2 + v_{i,j}^2}v_{i,j}) \end{bmatrix} \tag{12}$$

where

$$S = \left[\frac{(h_{i+1,j} - h_{i-1,j})}{2\Delta x}\frac{u_{i,j}}{\sqrt{u_{i,j}^2 + v_{i,j}^2}} + \frac{(h_{i,j+1} - h_{i,j-1})}{2\Delta y}\frac{v_{i,j}}{\sqrt{u_{i,j}^2 + v_{i,j}^2}}\right]A_{i,j}$$

We take the flow of ambient fluid over the dense, intruding gravity current to be analogous to water flowing over a blunt two-dimensional rigid body moving through deep water along a bottom surface. The body experiences a profile drag because of the relative motion (or dynamic pressure) of the ambient fluid. Strong turbulence along the current head may alter the 'dissipation' [17], but skin friction drag caused by turbulence is typically small compared with profile drag for flows over aircraft and ships. Technically the drag imposed by the ambient fluid is a function of local current height along the head region, however, for simplicity, we use a single drag coefficient for the entire head region.

The drag coefficient (front-capture method) has to be specified to account for 'unique' fluid physics occurring at the current head. The ambient fluid has a significant influence on the expansion of a gravity current, unless the ambient fluid density is small compared with the current. For example, this special treatment of the current front may not be necessary for the standard dam-break problem that involves an ambient-to-current density ratio of ~ 0.001 (i.e., air-to-water).

This drag term implicitly produces a diffuse representation of the front within the flow domain. The drag is applied in proportion to the exposed area. Since the finite volume cells in the current head are relatively more exposed than the cells inside the front, the leading-edge cells are more strongly decelerated by the relative wind. Thus, the head tends to form a shape with a large slope gradient at the leading edge (or front). The tendency for bluntness of the head is balanced by the hydrostatic pressure gradient that opposes this drag effect. The numerical simulations suggest that the *Fr* at the head is directly related to the drag force.

We can in fact derive an analytical expression for the dependence of *Fr* on the drag coefficient from application of the quasi-one-dimensional momentum equation to a homogeneous current along a level floor

$$\frac{\partial}{\partial t}\int_x (\rho_{\text{c}} hu)\,\mathrm{d}x + \oint_C (\rho_{\text{c}} hu^2 + (\rho_{\text{c}} - \rho_{\text{a}})gh^2/2)\hat{i}\cdot\mathrm{d}\vec{C} = \int_x (N_{\text{profile}} + N_{\text{friction}})\,\mathrm{d}x \tag{13}$$

We assume that the current head behaves as a rigid body intruding into an ambient fluid at a constant speed along the level slope. This seems reasonable since we observed in early simulations that after the initial collapse, a near-constant shape head forms, which diminishes in scale only gradually. Consequently, the dominant forces acting on the current head are gravity and profile drag. Acceleration, friction and momentum flux terms may be neglected to obtain

$$\oint_C ((\rho_c - \rho_a)gh^2/2)\hat{i}\cdot d\vec{C} = \int_x \left(\frac{\rho_a u^2 C_D}{2}\right)\frac{\partial h}{\partial x}\,dx \tag{14}$$

According to simulation results using the front-capture code, the velocity within the current increases rapidly from zero at the leading edge to a maximum value near the apex of the current head. Despite this velocity gradient, the momentum flux gradient in the moving reference frame is small compared with the gradients in the gravity and profile drag terms.

Applying Equation (14) to a moving control volume within the head region and near the apex of the current height, as in Figure 2, we obtain the following:

$$[(\rho_c - \rho_a)gh^2/2]_{x_1}^{x_2} = [\rho_a u^2 C_D h/2]_{x_1}^{x_2} \tag{15}$$

Expanding the terms and assuming an uniform velocity for the control volume

$$(\rho_c - \rho_a)g(h_2^2 - h_1^2) = \rho_a u^2 C_D(h_2 - h_1) \tag{16}$$

Introducing the reduced gravity definition ($g' = g(\rho_c - \rho_a)/\rho_a$) and an average current height ($h = (h_1 + h_2)/2$) leads to a simple expression for the head Fr as a function of drag coefficient

$$Fr = \frac{u}{\sqrt{g'h}} = \sqrt{\frac{2}{C_D}} \tag{17}$$

Equation (17) applies equally well to quasi-three-dimensional axisymmetric currents once the current has expanded to where the current radius is much larger than head length.

Figure 3 shows excellent agreement between the analytic result (Equation (17)) and numerical simulation results for axisymmetric currents provided the mesh is relatively fine. There is a small, monotonic increase in the head Fr during the numerical simulations because

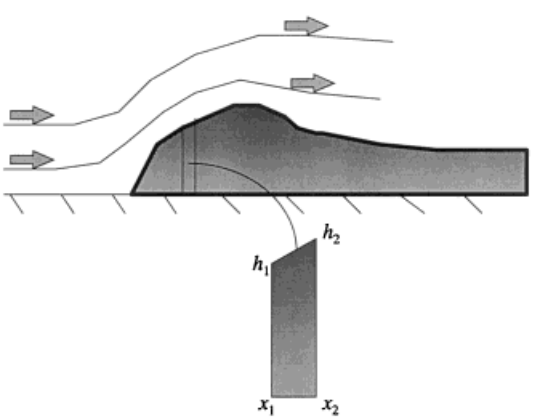

Figure 2. Current head schematic.

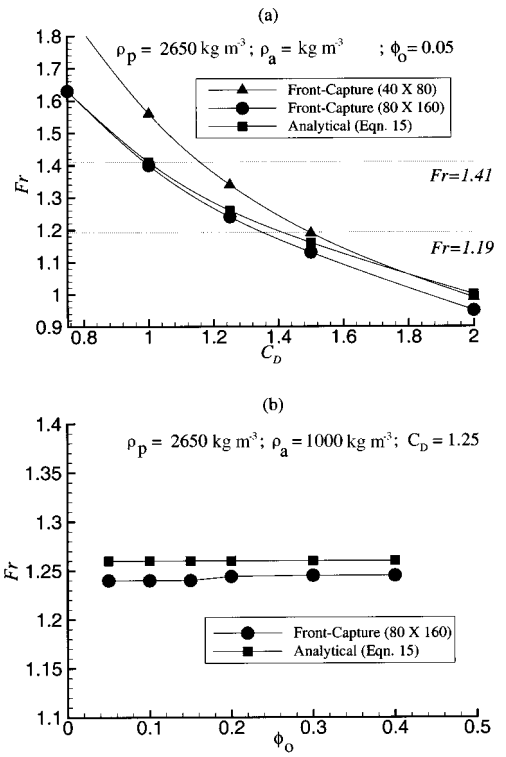

Figure 3. Head Froude vs (a) drag coefficient and (b) particle volume fraction for homogeneous, axisymmetric currents.

of a lack of resolution of the head region as the current expands. The *Fr* values in Figure 3 are taken after the current has 'settled' and before the head resolution becomes coarse. Dynamic mesh adaption in the head region would greatly reduce computational requirements by permitting a coarse mesh for the 'internal' flow.

Figure 3(a) indicates that C_D in the range of 1.0–1.4 results in a *Fr* range of approximately 1.4–1.2 for non-sloping, homogeneous, frictionless cases. Recall that this *Fr* range corresponds to values determined by previous researchers. The relationship between C_D and *Fr* is essentially unaffected by large changes in the current-to-ambient density ratios, as suggested by Figure 3(b).

The range of values of C_D is physically reasonable based on the bulbous shape of gravity current heads. For example, a blunt body in a turbulent, incompressible flow will produce a C_D of about 1.0. If there is separated flow behind the blunt body (or on the backside of the head region) C_D will increase; a cylinder in cross-flow will produce a C_D of about 1.2 in a strongly separated flow. The theoretical inviscid upper limit for the C_D is 2.0 (e.g., a flat plate in rarefied air). A C_D of less than 0.5 implies a sleek, three-dimensional shape. Consequently,

the calculated C_D range appears physically reasonable and may be chosen to produce a desired Fr for the non-sloping case. Specifically, we choose $C_D = 1.25$ plus a bed friction term, via a Manning coefficient, to approximate the experimental $Fr = 1.19$ during the code validation exercises.

6. CODE VALIDATION

We validated the new front-capture code on two different axisymmetric cases expanding along horizontal surfaces. Initial conditions for these cases are in Table I.

Time sequences of fluid height and velocity profiles for Case 1 are shown in Figures 4 and 5 respectively, using both codes. Each slice of data shown is taken along the x-axis for convenience. There is a negligible sensitivity of these profiles to which radial slice is taken from the solution (i.e., no directional dependence is evident). Overall agreement of the general shape of the current is excellent throughout the simulation for both variables. The front-capture scheme tends to diffuse (i.e., smear) the profiles somewhat because of the added numerical dissipation and the inherent nature of the scheme. The resolution of the mesh is 80×160 for the front-capture code (half-domain) and 80×80 for the front-tracking code (plus 4000 segments for the circular front).

Figure 6 illustrates the effect of mesh size on the current height profile for Case 1. The shape of the current head is 'sharpened' by increased mesh size since the front is captured over approximately the same number of cells in each case. However, the head location (e.g., mid-point between the apex and leading edge) and total volume are only slightly affected by mesh size. Later in the simulation (not shown) the effect of mesh size on head position is more pronounced. The coarse mesh solutions diverge due to a progressive loss of numerical resolution of the head region. As the current expands, the head region becomes a smaller percentage of the overall current radius and this error becomes progressively more important. Local, dynamic grid refinement near the front would alleviate this effect.

Case 2 was configured to validate the front-capture code for cases involving particle deposition. The simulations include three different particle types, each with a different settling velocity. The simulations are halted once the current deposited 99 per cent of the original, total

Table I. Axisymmetric source definition parameters for validation runs.

Parameter	Symbol	Case 1	Case 2
Initial shape	—	Disk	Disk
Initial current height (m)	h_0	20.0	20.0
Initial current radius (m)	r_0	40.0	40.0
Number of particle types	—	1	3
Initial particle volume fractions	ϕ_0	0.05	0.02, 0.02, 0.02
Ambient fluid density (kg m^{-3})	ρ_a	1000	1000
Particle densities (kg m^{-3})	ρ_p	2650	2650, 2650, 2650
Particle deposition	—	No	Yes
Particle settling velocities (cm s^{-1})	V_s	0.0	0.04, 2.0, 4.0

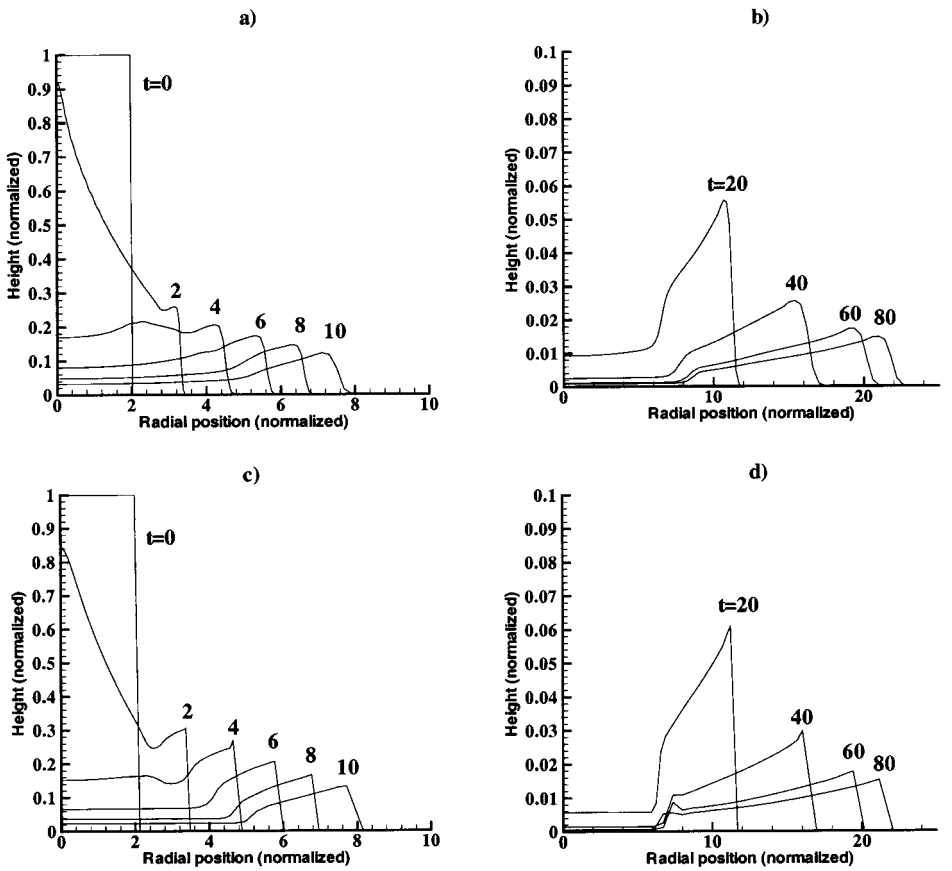

Figure 4. Current height profiles for Case 1 (a) front-capture during initial collapse, (b) front-capture during subsequent expansion, (c) front-tracking during initial collapse and (d) front-tracking during subsequent expansion.

particle mass. Again, excellent agreement was obtained for the current height and velocity profiles throughout the simulation (Figures 7 and 8) with some slight divergence very late in the run. Again, the data is extracted from a radial slice along the x-axis. No directional dependence in the axisymmetric solution is evident. The mesh resolutions are the same as in Case 1. The gravity current experiences a hydraulic jump within the head region because of a large gradient in current density at around 0.70 km after about 98 per cent of the particles have been deposited (not shown). Although both codes showed this hydraulic jump, a slightly weaker jump is predicted by the front-capture code.

Figure 9 illustrates the predicted areal density of the Case 2 deposit (i.e., particle mass deposited per unit area) versus radial position from the current source using both codes. Good

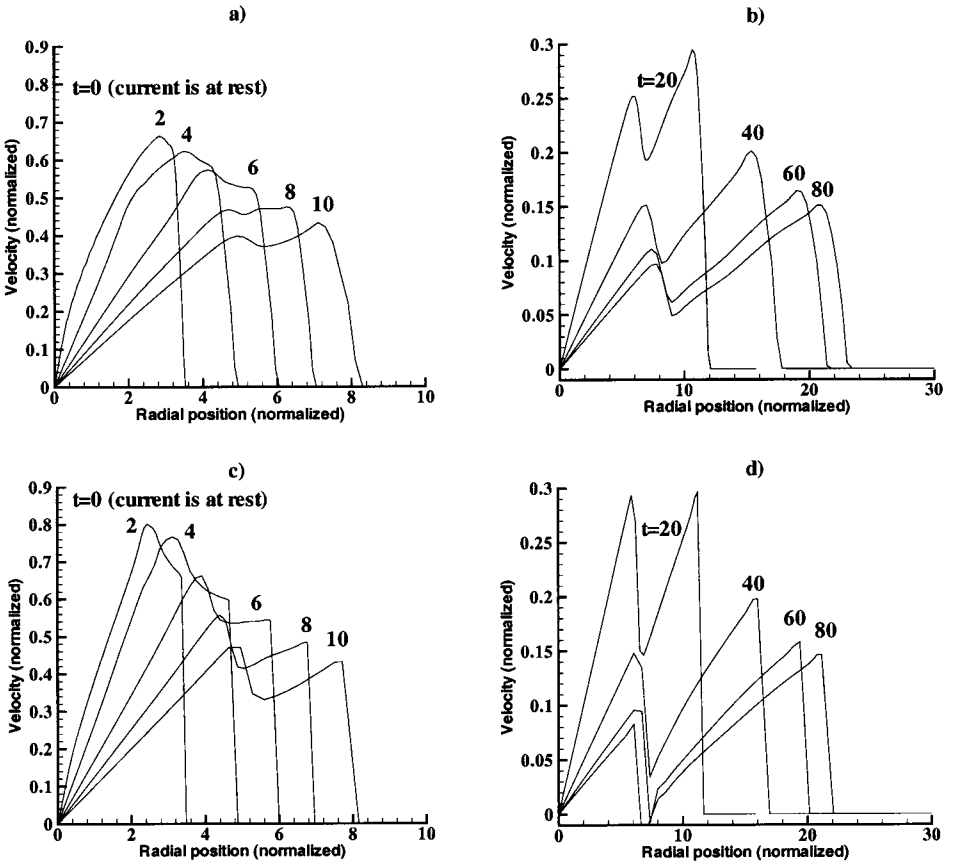

Figure 5. Current velocity profiles for Case 1 (a) front-capture during initial collapse, (b) front-capture during subsequent expansion, (c) front-tracking during initial collapse and (d) front-tracking during subsequent expansion.

qualitative and quantitative agreement exists. The modest differences near the origin ($r = 0$) are not significant when considering the total mass at a given radial position is proportional to r^2. The differences near the front, late in the simulations, also have a negligible effect on the difference between the final deposits.

Simulation results for both of these axisymmetric, expanding gravity currents resulted in essentially perfect concentric circle fronts at each time realization. However, for a large head Froude number (i.e., small profile drag coefficients) the fronts will become distorted because of a numerical 'preference' along the Cartesian axes. Alcrudo and Garcia-Navarro [18] have documented similar numerical behavior for dam-break problems involving a circular front initial condition and a Cartesian mesh.

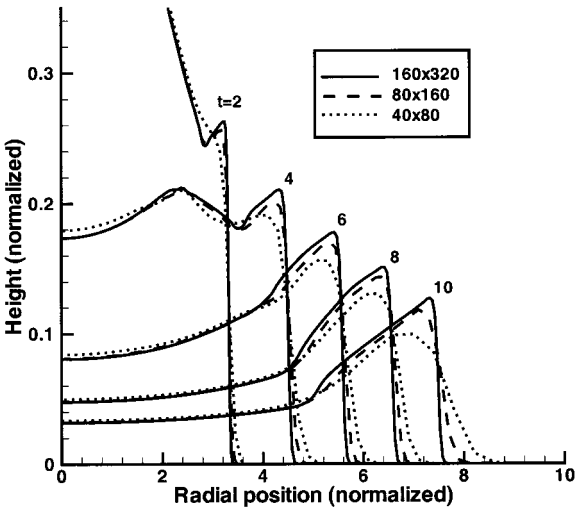

Figure 6. Effect of mesh size on Case 1 height profiles (front-capture during initial collapse).

7. FRONT-MERGING CAPABILITY

As discussed earlier, one of the main advantages of the new front-capture scheme over front-tracking schemes is the ability to easily handle merging fronts. Special and expensive numerical treatment is required with a front-tracking code. In contrast, the front-capture scheme simulates front merging with no additional programming effort. For example, Figure 10 shows a time sequence of the merging of two separate gravity currents at normalized time levels: $t^* = 0, 1, 2, 4, 8$. The sequence is as follows: (a) the initial condition (i.e., before release) for the two currents; (b) two fronts have started to expanding and about to merge; (c) the merged front has 'spiked'; (d) the new middle 'front' has been formed; and (e) the new front is expanding asymmetrically behind the original front. The contour levels, as well as the current outline, indicate the height distribution over the planar basin.

8. FLOW DOWN A PLANAR SLOPE

As discussed earlier, one of the primary objectives here was to develop a front-capture scheme that can simulate gravity flows over complex surfaces. We simulated the expansion of an initially axisymmetric source over a planar surface tilting downslope as a simple demonstration of this capability. Table II contains a list of the source parameters for this demonstration. The profile drag coefficient from the level slope cases is applied here—it is assumed that bulbous shape of the current head would persist. The simulation results show significant variation in the head Froude number along the current head. Consequently, it is not appropriate to apply a single Froude condition at the boundary, as is done within the front-tracking approach.

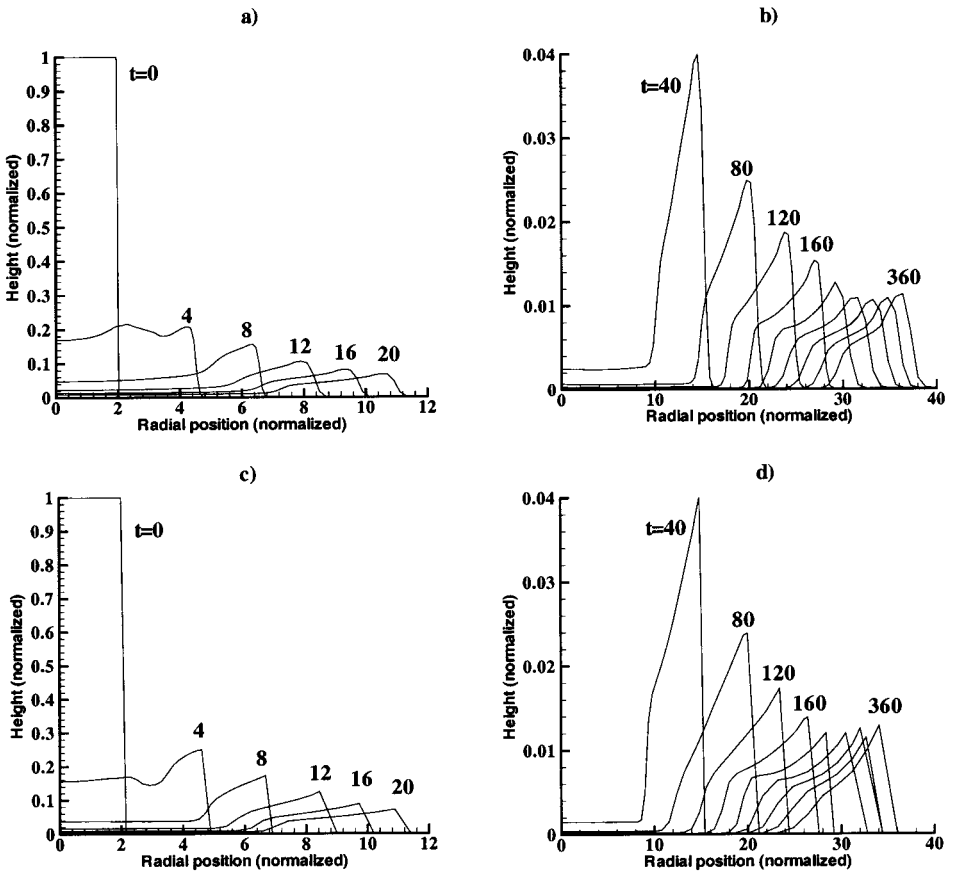

Figure 7. Current height profiles for Case 2 (a) front-capture during initial collapse, (b) front-capture during subsequent expansion, (c) front-tracking during initial collapse and (d) front-tracking during subsequent expansion.

Figure 11 shows a time sequence of the evolution of the gravity current source into the expected 'tear-drop' shape. The sequence includes the normalized time levels $t^* = 10$, 90, 170 and 250. The contour levels indicate the current height distribution. This sequence also illustrates the position of the current front boundaries as a function of time in plan view. Figure 12 illustrates the areal density of deposit distribution (i.e., the particle mass per unit area) at the end of the simulation, when 99 per cent of the particles have been deposited, using contours in plan view. It is clear than even a small downslope angle (i.e., 0.5°) has a dramatic influence on current development and the deposit distribution. This demonstration is a precursor to future work in which gravity flows over both simple and complex surfaces will be studied.

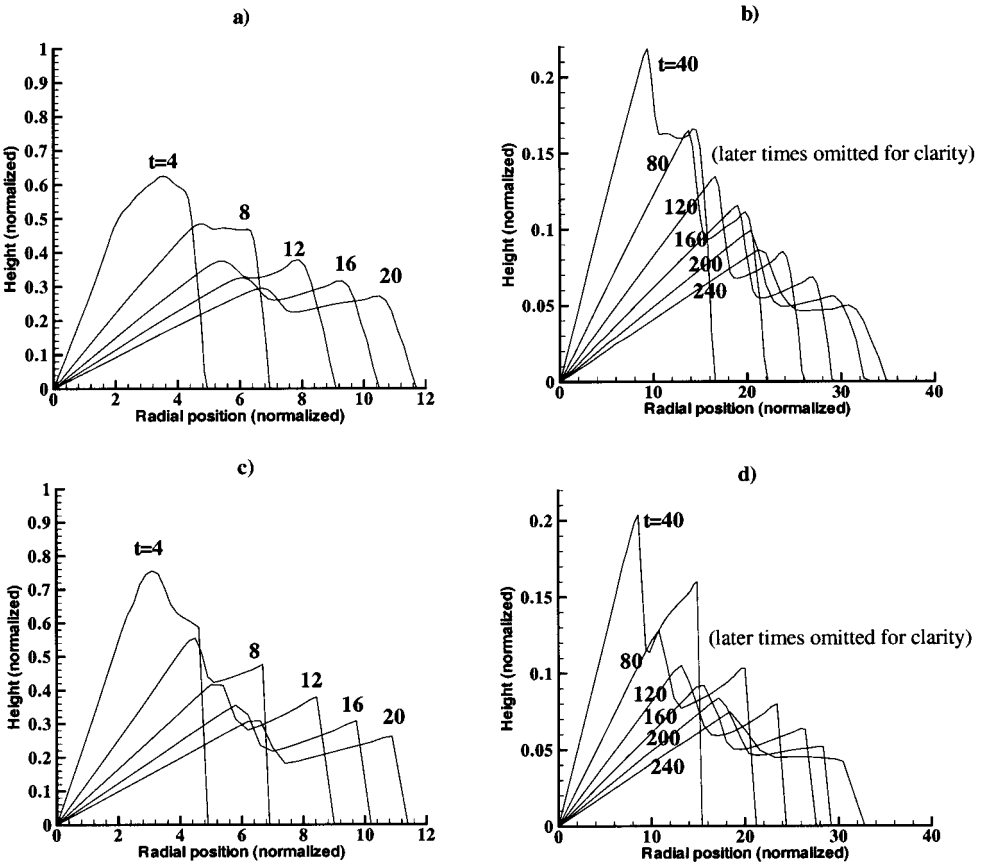

Figure 8. Current velocity profiles for Case 2 (a) front-capture during initial collapse, (b) front-capture during subsequent expansion, (c) front-tracking during initial collapse and (d) front-tracking during subsequent expansion.

In order to ensure numerical stability the scheme was modified to maintain a 'thin film' of current throughout the computational domain. If the current height drops below this pre-defined level, the current height is simply reset to the tolerance value. The thin film value used in the downslope simulation is 0.0001 times the original source height. The film contains a negligible amount of particle mass. This occurs for the downslope problem, for example, because the current along the shelf wall eventually moves down the slope. Although this modification violates the conservation of source particle mass, the effect of maintaining a thin film on the simulation results can be neglected.

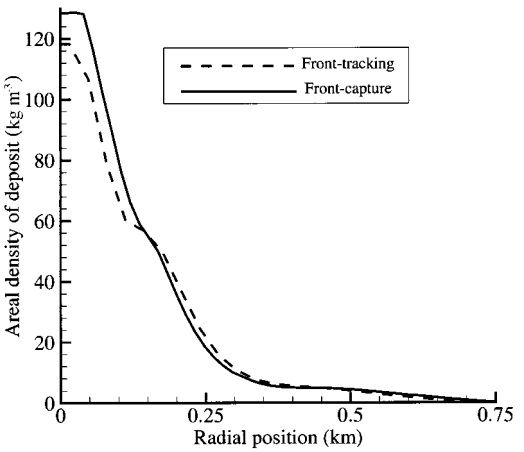

Figure 9. Final particle mass deposit distributions for Case 2 (front-capture vs front-tracking).

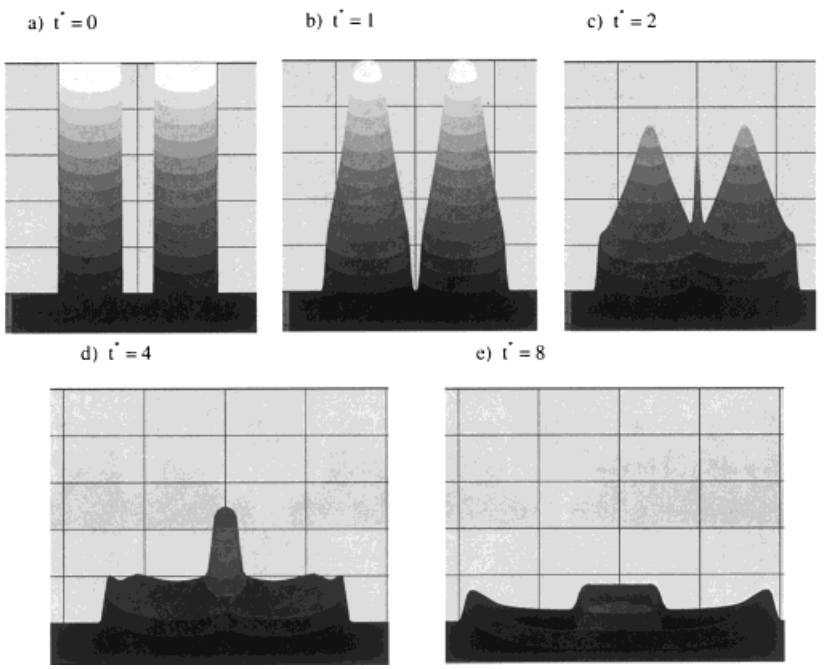

Figure 10. Time sequence of merging fronts (a) initial condition, (b) fronts about to merge, (c) merging initiated, (d) middle front formed, (e) continued expansion of merged front.

Table II. Axisymmetric source definition parameters for flow down a planar slope

Parameter	Symbol	Case 3
Initial shape	—	Disk
Initial current height (m)	h_0	20.0
Initial current radius (m)	r_0	40.0
Number of particle types	—	1
Initial particle volume fractions	ϕ_0	0.05
Ambient fluid density (kg m^{-3})	ρ_a	1000
Particle densities (kg m^{-3})	ρ_p	2650
Particle deposition	—	Yes
Particle settling velocities (cm s^{-1})	V_s	0.04
Downslope (°)	θ	0.5

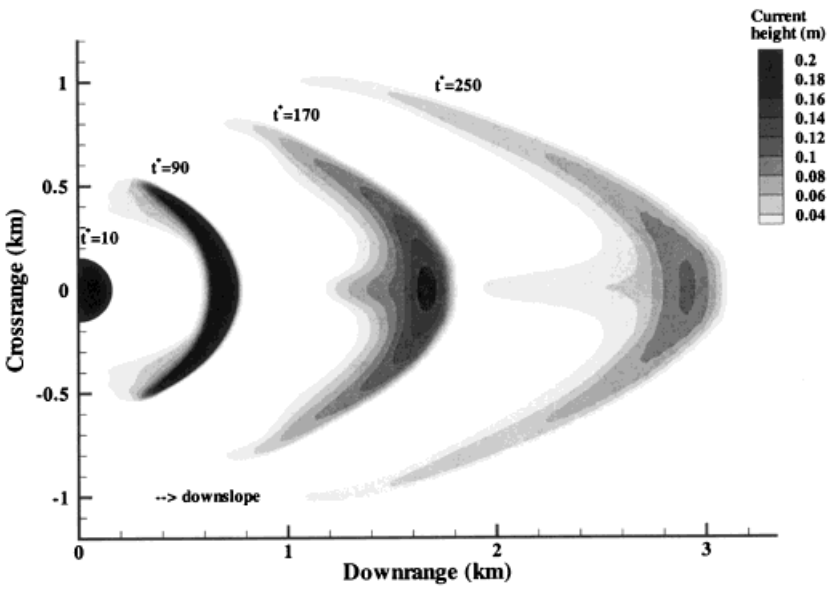

Figure 11. Time sequence of flow down a planar slope due to an axisymmetric source at four realizations: $t^* = 10$, 90, 170 and 250.

9. CONCLUSIONS

We present a new scheme for the simulation of gravity currents over complex surfaces using augmented shallow water wave equations. The current front is captured implicitly by estimating the profile drag exerted by the ambient fluid on the intruding gravity current. Capturing the front based on appropriate fluid physics, rather than imposing a single Froude condition,

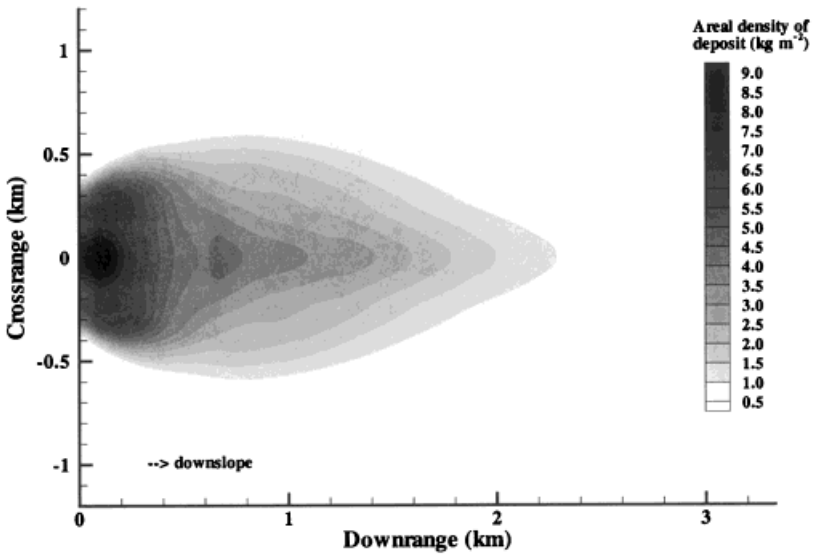

Figure 12. Areal density of deposit contours after 99 per cent of particles have been deposited by the particle-laden flow down a planar slope.

is a necessary step towards a general, gravity current simulation capability. The proposed scheme has also been formulated to ensure numerical stability during the expansion process.

A physically reasonable profile drag coefficient results in an appropriate head Froude number for the non-sloping case—evidence that the physical model is correct. The head Fr is set by a balance between the hydrostatic pressure gradient and the profile drag. A simple analytical expression is derived for the head Fr as a function of the profile drag coefficient for the non-sloping case.

The new scheme provides an efficient and reasonably accurate means of simulating gravity currents without excessive programming effort (as with front-tracking methods) or excessive computational cost (as with full three-dimensional solutions). The capability of the new scheme to simulate the flow of homogeneous and non-homogenous gravity currents over a level basal surface is verified, as is the capability to simulate merging fronts and flows down mild slopes.

REFERENCES

1. Simpson JE. *Gravity Currents in the Environment and the Laboratory*. Ellis Horwood: Chichester, 1987.
2. Wesser OE. Deep-water oil sand reservoirs-ancient case histories and modern concepts. AAPG Continuing Education Course Notes Series No. 6, 1977.
3. Mutti E. *Turbiditic Sandstones*. Instituto di Geologia, Universita di Parma: Parma, 1992.
4. Karman TV. The engineer grapples with nonlinear problems. *Bulletin of the American Machine Society* 1940; **46**: 615–683.
5. Benjamin TB. Gravity currents and related phenomenon. *Journal of Fluid Mechanics* 1968; **31**: 209–248.
6. Huppert HE, Simpson JE. The slumping of gravity currents. *Journal of Fluid Mechanics* 1980; **99**: 785–799.

7. Bonnecaze RT, Huppert HE, Lister JR. Particle-driven gravity currents. *Journal of Fluid Mechanics* 1993; **250**: 339–369.
8. Bonnecaze RT, Hallworth MA, Huppert HE, Lister JR. Axisymmetric particle-driven gravity currents. *Journal of Fluid Mechanics* 1995; **294**: 93–121.
9. Bonnecaze RT, Huppert HE, Lister JR. Patterns of sedimentation from polydispersed turbidity currents. *Proceedings of the Royal Society A* 1996; **452**: 2247–2261.
10. Sparks RSJ, Bonnecaze RT, Huppert HE, Lister JR, Mader H, Hallworth MA, Phillips J. Sediment-laden gravity currents with reversing buoyancy. *Earth and Planetary Science Letters* 1996; **114**: 243–257.
11. Bonnecaze RT, Lister JR. Particle-driven gravity currents down planar slopes. *Journal of Fluid Mechanics* 1999, in press.
12. Whitaker S. *Introduction to Fluid Mechanics* (3rd edn). Kreiger Publishing: Malabar, FL, 1984; 349–353.
13. Shu C, Osher S. Efficient implementation of essentially non-oscillatory shock-capturing schemes. *Journal of Computational Physics* 1988; **77**: 439–471.
14. Nujic M. Efficient implementation of non-oscillatory schemes for the computation of free-surface flows. *Journal of Hydraulic Research* 1995; **33**(1): 101–111.
15. Nessyahu H, Tadmor E. Non-oscillatory central differencing for hyperbolic conservation laws. *Journal of Computational Physics* 1990; **87**: 408–463.
16. Chern IL, Glimm J, McBryan O, Plohr B, Yaniv S. Front tracking for gas dynamics. *Journal of Computational Physics* 1986; **62**: 83–110.
17. Garvine RW. Frontal jump conditions for models of shallow, buoyant surface layer hydrodynamics. *Tellus* 1981; **33**: 301–312.
18. Alcrudo F, Garcia-Navarro P. A high resolution Godunov-type scheme in finite volumes for the 2D shallow-water equations. *International Journal for Numerical Methods in Fluids* 1993; **16**: 489–505.

